# QCD critical point from the Nambu–Jona-Lasino model with a scalar-vector interaction

Kai-Jia Sun[*] and Che Ming Ko[†]

*Cyclotron Institute and Department of Physics and Astronomy, Texas A&M University, College Station, Texas 77843, USA*

Shanshan Cao[‡]

*Cyclotron Institute, Texas A&M University, College Station, Texas 77843, USA and Department of Physics and Astronomy, Wayne State University, Detroit, Michigan 48201, USA*

Feng Li[§]

*School of Physical Science and Technology, Lanzhou University, Lanzhou, Gansu 073000, China*

We study the critical point in the QCD phase diagram in the Nambu–Jona-Lasino (NJL) model by including a scalar-vector coupled interaction. We find that varying the strength of this interaction, which has no effect on the vacuum properties of QCD, can significantly affect the location of the critical point in the QCD phase diagram, particularly the value of the critical temperature. This provides a convenient way to use the NJL-based transport or hydrodynamic model to extract information about the QCD phase diagram from relativistic heavy-ion collisions.

## I. INTRODUCTION

Studying the QCD phase structure is among the most important goals of ongoing experiments on heavy-ion collisions [1–3]. By changing the beam energy and selecting different system sizes and the rapidities of measured particles, it is possible to probe different regions of the QCD phase diagram, particularly the critical end point (CEP) [4] on the first-order phase transition line. To make this possible requires, however, versatile dynamic models to describe the expansion of created hot dense matter with a flexible equation of state that can have the critical point at varying temperatures ($T$) and baryon chemical potentials ($\mu_B$) in the QCD phase diagram [5–15].

At zero and small baryon chemical potentials, the lattice quantum chromodynamics (LQCD) [16–18] has shown that the quark-gluon plasma (QGP) to hadronic matter phase transition is a smooth crossover. However, it is not yet possible for the lattice QCD to study the quark-hadron phase transition at large baryon chemical potentials due to the fermion sign problem. On the other hand, studies based on effective theories have suggested that the phase transition is a first-order one at large baryon chemical potentials [4,19–25], indicating the existence of a CEP on

the first-order phase transition line in the $\mu_B - T$ plane of the QCD phase diagram, albeit with large uncertainties in its location [23].

Among the effective models for studying the QCD phase diagram at finite baryon chemical potentials, a frequently used one is the Nambu–Jona-Lasinio model [26,27]. Formulated in terms of quark degrees of freedom [28,29], this model allows the description of chiral phase transition at both finite temperature and chemical potential [30] besides providing a framework to describe hadronic systems in the vacuum based on dynamical chiral symmetry breaking and its restoration [31–33]. The extended NJL model with the Polyakov-loop (PNJL) also makes it possible to describe the confinement-deconfinement phase transition of the quark matter [20,34–40]. The parameters in the NJL model and the PNJL model are largely constrained by the vacuum properties of QCD and the known chiral dynamics in hadronic systems at zero temperature. The predicted temperature of the critical point varies from 40 to 80 MeV in the NJL model [23,30] and can be larger than 100 MeV in the PNJL model [40,41]. For the purpose of locating the critical point via comparing model calculations with the experimental data from heavy-ion collisions, it will be useful to extend the NJL-type models to further expand the region in the $\mu_B - T$ plane, where possible locations of the critical point can be accommodated.

Although a repulsive vector interaction can be included in the NJL or PNJL model to change the critical temperature of

[*]kjsun@tamu.edu
[†]ko@comp.tamu.edu
[‡]shanshan.cao@wayne.edu
[§]fengli@lzu.edu.cn

the chiral and/or deconfinement phase transition [20], it, however, leads to a decrease of the critical temperature, making the deviation from the LQCD results even larger [42]. Another way to extend the NJL model is to include higher-order multiquark interactions. Besides the six-quark interaction term from the 't Hooft determinant interaction that breaks the $U_A(1)$ symmetry [43], the eight-quark interactions, including scalar-scalar, vector-vector, and scalar-vector coupled interaction terms, have also been considered [44–46]. These higher-order interactions are produced from quantum effects in the high momentum region of the nonperturbative renormalization group calculation [47]. Their possible effects on the vacuum properties of low-lying spin zero mesonic spectra have been carefully studied in Refs. [48–50]. In addition, the inclusion of a complete set of spin zero terms from explicit symmetry breaking effects [51,52] has led to a more precise description of low-lying pseudoscalar and scalar nonets as well as a good description of a wide range of observables from LQCD calculations [53].

Since the attractive scalar-scalar coupled interaction affects the QCD vacuum properties, its strength is constrained and cannot be arbitrarily changed to modify the location of the critical point [45]. Although the repulsive vector-vector coupled interaction does not affect the QCD vacuum properties, it always decreases the critical temperature of baryon-rich quark matter, similar to the effect of the vector interaction. For the scalar-vector coupled interaction, it is known to be important for reproducing the nuclear saturation properties when using the NJL-type model for nuclear matter [54]. As to its application to the quark-hadron phase transition [55], it turns out to be a good candidate because it has no effects on the QCD vacuum properties, and more importantly, its strength can affect the location of the critical point as shown below. By varying the strength of the scalar-vector coupled interaction, one can easily change the location of the critical point in the phase diagram from low to very high temperatures. These features of the scalar-vector coupled interaction term have not been fully explored in previous studies [44–46,51–53].

In the present study, we first calculate the phase diagram from the two-flavor NJL model by including the scalar-vector coupled interaction among quarks. We then extend the calculations to the three-flavor case and also to the PNJL model to study in detail its effect on the location of the critical point in the QCD phase diagram.

## II. THE SCALAR-VECTOR COUPLED INTERACTION IN THE (P)NJL MODEL

### A. The two-flavor NJL model

We first consider the two-flavor NJL model, which is usually described by the following Lagrangian density [30]:

$$\mathcal{L}_{\mathrm{NJL}}^{\mathrm{SU}(2)} = \mathcal{L}_0 + \mathcal{L}_{\mathrm{S}} + \mathcal{L}_{\mathrm{SV}}, \tag{1}$$

with

$$
\begin{aligned}
\mathcal{L}_0 &= \bar{\psi}(i\gamma^\mu \partial_\mu - \hat{m})\psi, \\
\mathcal{L}_{\mathrm{S}} &= G_S[(\bar{\psi}\psi)^2 + (\bar{\psi}i\gamma_5\vec{\tau}\psi)^2], \\
\mathcal{L}_{\mathrm{SV}} &= G_{\mathrm{SV}}[(\bar{\psi}\psi)^2 + (\bar{\psi}i\gamma_5\vec{\tau}\psi)^2] \\
&\quad \times [(\bar{\psi}\gamma^\mu\psi)^2 + (\bar{\psi}\gamma_5\gamma^\mu\vec{\tau}\psi)^2].
\end{aligned}
\tag{2}
$$

In the above, $\psi = (u, d)^T$ represents the two-flavor quark fields, $\hat{m} = \mathrm{diag}(m_u, m_d)$ is the current quark mass matrix, $\gamma^\mu$ with $\mu = 0, 1, 2, 3$ are Dirac matrices, $\gamma_5 = i\gamma_0\gamma_1\gamma_2\gamma_3$, and $\vec{\tau} = (\tau_1, \tau_2, \tau_3)$ are Pauli matrices in the flavor space. The Lagrangian densities $\mathcal{L}_0$, $\mathcal{L}_{\mathrm{S}}$, and $\mathcal{L}_{\mathrm{SV}}$ are, respectively, for the free quarks and their scalar and pseudoscalar interactions with the coupling constant $G_S$ as well as the scalar-vector, scalar-axial vector, pseudoscalar-vector, and pseudoscalar-axial vector coupled interactions with the coupling constant $G_{\mathrm{SV}}$. We note that the sign of the $G_{\mathrm{SV}}$ term in Eq. (2) is the same as the one first introduced in Ref. [54], which is opposite to that used in Refs. [45,55].

As in most studies using the NJL model, we adopt the mean-field approximation [56] to linearize the model by introducing following substitutions:

$$
\begin{aligned}
(\bar{\psi}\Gamma_i\psi)^2 &= 2\bar{\psi}\Gamma_i\psi\langle\bar{\psi}\Gamma_i\psi\rangle - \langle\bar{\psi}\Gamma_i\psi\rangle^2 \\
(\bar{\psi}\Gamma_i\psi\bar{\psi}\Gamma_j\psi)^2 &= \langle\bar{\psi}\Gamma_i\psi\rangle^2(2\bar{\psi}\Gamma_j\psi\langle\bar{\psi}\Gamma_j\psi\rangle) \\
&\quad + \langle\bar{\psi}\Gamma_j\psi\rangle^2(2\bar{\psi}\Gamma_i\psi\langle\bar{\psi}\Gamma_i\psi\rangle) \\
&\quad - 3\langle\bar{\psi}\Gamma_i\psi\rangle^2\langle\bar{\psi}\Gamma_j\psi\rangle^2,
\end{aligned}
\tag{3}
$$

where $\Gamma = \{1, i\gamma_5\vec{\tau}, \gamma_\mu, \gamma_5\gamma_\mu\}$ and the angular bracket denotes the expectation value from the quantum-statistical average. Due to the parity symmetry in a static quark matter, one has $\langle\bar{\psi}\gamma^k\psi\rangle = \langle\bar{\psi}\gamma_5\vec{\tau}\psi\rangle = \langle\bar{\psi}\gamma_5\gamma^\mu\psi\rangle = 0$ with $k = 1, 2, 3$, and the Lagrangian density can then be rewritten as

$$
\begin{aligned}
\mathcal{L}_{\mathrm{NJL}}^{\mathrm{SU}(2)} &= \bar{u}(\gamma^\mu i\partial_{u\mu} - M_u)u + \bar{d}(\gamma^\mu i\partial_{d\mu} - M_d)d \\
&\quad + 2G_{\mathrm{SV}}(\rho_u + \rho_d)(\phi_u + \phi_d)^2(\bar{u}\gamma^0 u + \bar{d}\gamma^0 d) \\
&\quad - G_S(\phi_u + \phi_d)^2 - 3G_{\mathrm{SV}}(\phi_u + \phi_d)^2(\rho_u + \rho_d)^2.
\end{aligned}
\tag{4}
$$

In the above, $M_u$ and $M_d$ are the in-medium effective masses of $u$ and $d$ quarks, respectively, given by

$$
\begin{aligned}
M_u &= m_u - 2G_S(\phi_u + \phi_d) \\
&\quad - 2G_{\mathrm{SV}}(\rho_u + \rho_d)^2(\phi_u + \phi_d), \\
M_d &= m_d - 2G_S(\phi_u + \phi_d) \\
&\quad - 2G_{\mathrm{SV}}(\rho_u + \rho_d)^2(\phi_u + \phi_d),
\end{aligned}
\tag{5}
$$

with $\phi_u = \langle\bar{u}u\rangle$ and $\phi_d = \langle\bar{d}d\rangle$ being the $u$ and $d$ quark condensates, respectively, and $\rho_u$ and $\rho_d$ denoting the net $u$ and $d$ quark number densities, respectively.

The thermodynamic properties of a two-flavor quark matter are determined by the partition function $\mathcal{Z} = \text{Tr}[\exp[-\beta(\hat{H} - \mu\hat{N})]]$, where $\beta = 1/T$ and $\hat{H}$ are, respectively, the inverse of the temperature $T$ and the Hamiltonian operator, and $\mu$ and $\hat{N}$ are, respectively, the chemical potential and corresponding conserved charge number operator. The thermodynamic grand potential of the quark matter is then given by

$$\begin{aligned}
\Omega_{\text{NJL}}^{\text{SU(2)}} &= -\frac{1}{\beta V}\ln\mathcal{Z} \\
&= G_S(\phi_u + \phi_d)^2 + 3G_{\text{SV}}(\phi_u + \phi_d)^2(\rho_u + \rho_d)^2 \\
&\quad - 2N_C \sum_{i=u,d} \int \frac{d^3p}{(2\pi)^3} E_i \\
&\quad - 2T \sum_{i=u,d} \int \frac{d^3p}{(2\pi)^3} (z^+(E_i) + z^-(E_i)),
\end{aligned}$$
(6)

where $V$ is volume of the system, $N_C = 3$ is the number of colors, $E_i = (m_i^2 + \mathbf{p}^2)^{1/2}$, and

$$z^{\pm}(E_i) = N_c \ln[1 + e^{-\beta(E_i \mp \mu_i^*)}],$$
(7)

with the effective chemical potentials,

$$\begin{aligned}
\mu_u^* &= \mu_u + 2G_{\text{SV}}(\rho_u + \rho_d)(\phi_u + \phi_d)^2, \\
\mu_d^* &= \mu_d + 2G_{\text{SV}}(\rho_u + \rho_d)(\phi_u + \phi_d)^2.
\end{aligned}$$
(8)

The quark condensate $\phi_i$ and the net quark number density $\rho_i$ can be determined by minimizing the grand potential, i.e.,

$$\frac{\partial\Omega_{\text{NJL}}^{\text{SU(2)}}}{\partial\phi_i} = \frac{\partial\Omega_{\text{NJL}}^{\text{SU(2)}}}{\partial\rho_i} = 0,$$
(9)

and they are

$$\phi_i = 2N_C \int \frac{d^3p}{(2\pi)^3} \frac{M_i}{E_i}(n_i^+ + n_i^- - 1),$$
(10)

$$\rho_i = 2N_C \int \frac{d^3p}{(2\pi)^3}(n_i^+ - n_i^-),$$
(11)

with $n_i^{\pm} = [e^{\beta(E_i \mp \mu_i^*)} + 1]^{-1}$. Because the NJL model is a nonrenormalizable effective model, a momentum cutoff $\Lambda$ is needed in evaluating the momentum integral in Eqs. (6), (10) and (11) as well as those appearing later in the paper. In the present study, we employ the parameters $m_u = m_d = 5.5$ MeV, $G_S\Lambda^2 = 2.135$, and a cutoff $\Lambda = 651$ MeV [39,40], which are summarized in Table I together with the quark in-medium mass and condensate, to study the QCD phase diagram with various values for $G_{\text{SV}}$.

TABLE I. Parameters in the two-flavor NJL model [39,40].

| $\Lambda$ [MeV] | $G_S\Lambda^2$ | $m_{u,d}$ [MeV] | $M_{u,d}$ [MeV] | $\langle\bar{u}u\rangle^{1/3}$ [MeV] |
|---|---|---|---|---|
| 651 | 2.135 | 5.5 | 325.1 | −251.3 |

With the quark condensates and net quark density given in the above, one can see from Eqs. (5) and (8) that the $G_{\text{SV}}$ term affects the effective masses of quarks and their effective chemical potentials in a quark matter. Although its effects depend on the quark condensates, which have negative values and increase with decreasing quark density, they also depend on the quark density. As a result, including the $G_{\text{SV}}$ term in the NJL model does not affect its description of QCD vacuum properties at zero baryon density, and treating the value of $G_{\text{SV}}$ as a free parameter allows one to obtain different scenarios for the properties of quark matter.

The effects of the $G_{\text{SV}}$ term can be qualitatively understood for quark matter at low density. According to Eq. (8), a negative $G_{\text{SV}}$ resembles a vector interaction in the NJL model [30], which induces a repulsive interaction among quarks or antiquarks and an attractive interaction between quark and antiquark. Compared to the scalar coupled term $G_S$ in the NJL model, which reduces the quark in-medium masses because of the reduction of quark condensates, a negative $G_{\text{SV}}$ counteracts this effect as can be seen from Eq. (5). With its quadratic dependence on the quark density, the effect of the $G_{\text{SV}}$ term on the quark in-medium masses at low quark densities is, however, significantly reduced with increasing quark density, thus resulting in an effectively attractive interaction among quarks. Since the repulsive quark interaction due to a negative $G_{\text{SV}}$ in the vector channel turns out to be stronger than the attractive quark interaction in the scalar channel for quark matter at low densities, the net effect of a negative $G_{\text{SV}}$ is repulsive. In quark matter at very high densities, where the chiral symmetry is largely restored and the quark condensates are close to zero, the effects of the $G_{\text{SV}}$ term become less important, which is different from the usual vector interaction in the NJL model [30] that gets stronger at high densities. For quark matter at intermediate densities, the effects of the $G_{\text{SV}}$ term are, however, more complex, and whether this leads to a repulsive or an attractive quark interaction depends on the value of the quark density. For a positive $G_{\text{SV}}$, its effects on the properties of quark matter are opposite to those of a negative $G_{\text{SV}}$.

Quantitatively, the effects of the $G_{\text{SV}}$ term on the properties of quark matter can be understood from its pressure, which is given by $p = -\Omega_{\text{NJL}}^{\text{SU(2)}}$, as a function of the net quark number density. In Fig. 1, we show the results for quark matter at temperature $T = 36$ MeV, which is the critical temperature in the two-flavor NJL model for $G_{\text{SV}} = 0$, for different values of the scalar-vector coupling constant $G_{\text{SV}}$. It is seen that a positive $G_{\text{SV}} = 100 \, \Lambda^{-8}$
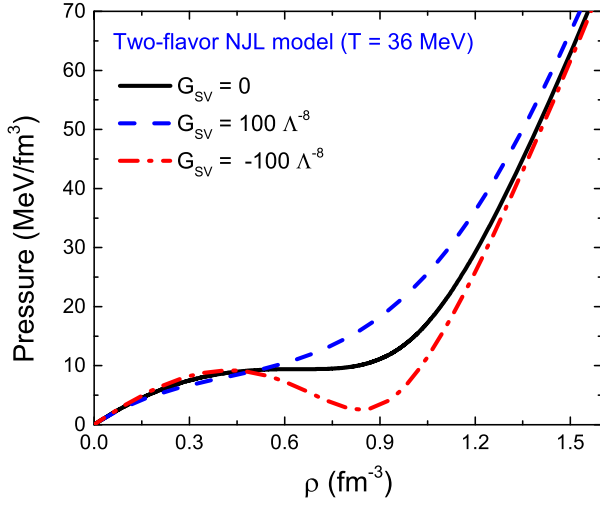
FIG. 1. Pressure as a function of net quark number density at temperature $T = 36$ MeV from the two-flavor NJL model for different values of the scalar-vector coupling constant $G_{SV}$ and with the values of other parameters given in Table I.

hardens the equation of state at net quark number density of around 0.9 fm$^{-3}$, while a negative $G_{SV} = -100 \Lambda^{-8}$ has the opposite effects. As a result, the critical temperature is increased by a negative $G_{SV}$ and decreased by a positive $G_{SV}$.

Figure 2 shows the coexistence line in the temperature and net quark number density plane for different values of $G_{SV}$. For points on the coexistence line that have the same temperature, they correspond to quark matters of different densities but the same pressure and chemical potential. The region below the coexistence line is unstable against phase separation. The blue solid line is the result calculated with $G_{SV} = 0$, i.e., the default NJL model, and
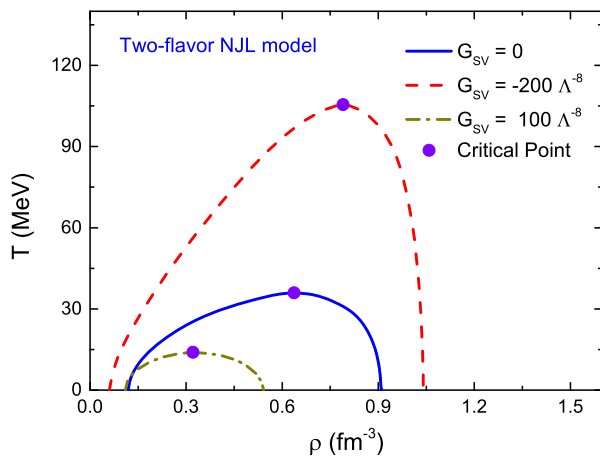
the corresponding critical point is located at temperature $T \approx 36$ MeV and net quark number density $\rho \approx 0.64$ fm$^{-3}$. Results obtained with a scalar-vector coupled interaction of $G_{SV} = -200 \Lambda^{-8}$ are shown by the dashed line, and the critical point in this case shifts to the temperature $T \approx 105.5$ MeV and net quark density $\rho \approx 0.79$ fm$^{-3}$. Changing to a scalar-vector coupled interaction of $G_{SV} = 100 \Lambda^{-8}$ reduces the temperature and net quark number density of the critical point to $T \approx 14$ MeV and $\rho \approx 0.32$ fm$^{-3}$, respectively. Hence, the critical temperature can be easily varied by changing the value of $G_{SV}$. The locations of the critical point obtained from the two-flavor NJL model for different values of $G_{SV}$ are also shown in Fig. 3 by the red line. Although it is not possible to obtain a critical point near the $\mu_B = 0$ axis by further reducing the value of $G_{SV}$, because its effects on the effective mass and chemical potential vanish at $\mu_B = 0$, the range of values for the critical temperature shown in Fig. 2 by varying $G_{SV}$ is sufficiently large to cover the region that can be probed in realistic heavy-ion collisions.

The value of $G_{SV}$ affects not only the location of the CEP but also the growth rate $\gamma_k$ of spinodal unstable modes in the phase coexistence region. The latter is related via the relation $\gamma_k = |v|k$, where $k$ is the wave number of the density ripples [57], to the isothermal speed of sound $v$ that is purely imaginary and thus corresponds to a nonpropagating and self-amplified sound wave. With the square of the speed of sound evaluated according to $v^2 = \frac{\rho}{\epsilon + p}(\frac{\partial p}{\partial \rho})_T$ in terms of the net quark density $\rho$ and the quark energy density $\epsilon$ and pressure $p$, its values as a function of $\rho$ in a quark matter of temperature $T = 30$ MeV are shown by the



FIG. 2. Coexistence lines in the temperature and net quark number density plane from the two-flavor NJL model for different values of the scalar-vector coupling constant $G_{SV}$ and with the values of other parameters given in Table I. The solid circles denote corresponding critical points.
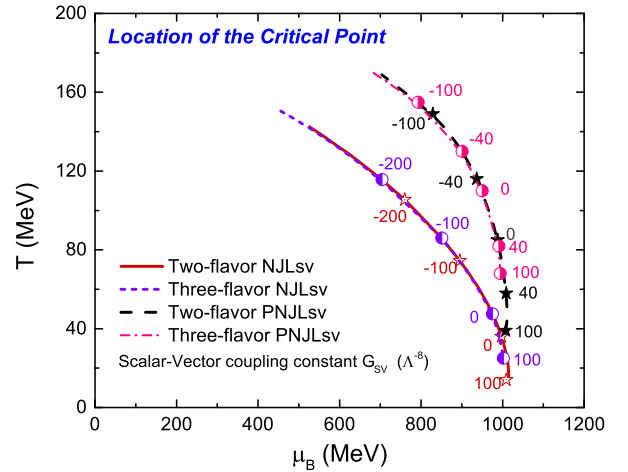


FIG. 3. Location of the critical point in two-flavor and three-flavor NJL models and PNJL models with the scalar-vector coupled interaction in the plane of temperature $T$ and baryon chemical potential $\mu_B$. The lines are obtained by changing the value of the coupling constant $G_{SV}$ with other parameters in the two-flavor and three-flavor (P)NJL models given in Table I and Table II, respectively.
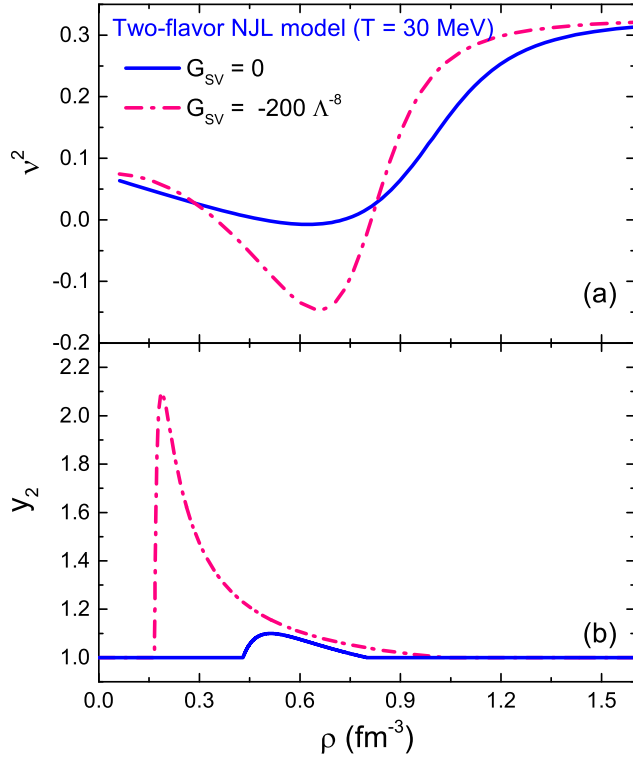
FIG. 4. Panel (a): square of sound velocity ($v^2$) in the two-flavor NJL model. Panel (b): second-order scaled density moment ($y_2$) obtained from the Maxwell construction of a first-order phase transition in quark matter.

solid and dashed lines in the upper panel of Fig. 4 for the quark scalar-vector interaction strength $G_{SV}$ equal to 0 and $-200 \, \Lambda^{-8}$, respectively. It is seen that in the spinodal unstable region defined by $(\frac{\partial p}{\partial \rho})_T < 0$, a negative-valued $G_{SV}$ leads to a more negative $v^2$, corresponding to a larger growth rate of spinodal unstable modes and hence, a faster phase separation.

Both the size of the phase-coexistence region in the QCD phase diagram and the growth rate of spinodal unstable modes can affect the observation of the first-order phase transition in heavy-ion collisions. This is because it requires the phase trajectory of produced quark matter to pass through the phase-coexistence region in the QCD phase diagram and the rapid development of fluctuations in density in order for clusters to form [57–59] and light nuclei to be more easily produced [59]. Therefore, a negative $G_{SV}$ makes the signals of a first-order phase transition more prominent in the simulations of heavy-ion collisions based on either the hydrodynamic or the transport approach.

To quantify the density inhomogeneity/fluctuation in quark matter, we consider the $N$th order scaled density moments [57], i.e.,

$$y_N = \frac{[\int d\mathbf{x}\rho(\mathbf{x})]^{N-1}[\int d\mathbf{x}\rho^{(N+1)}(\mathbf{x})]}{[\int d\mathbf{x}\rho^2(\mathbf{x})]^N}, \quad (12)$$

which has a value of one for a uniform density distribution. For small density fluctuations, $\rho(\mathbf{x}) = \rho_0 + \delta\rho(\mathbf{x})$ with $\rho_0$ being the average density, it can be written as

$$y_2 \approx 1 + \frac{\int d\mathbf{x}(\delta\rho(\mathbf{x}))^2}{\int d\mathbf{x}\rho_\mathbf{0}^2} \equiv 1 + \Delta\rho, \quad (13)$$

in terms of the relative density fluctuation $\Delta\rho$ averaged over space [60,61]. As shown in Refs. [59–62], the quantities $y_2$ and $\Delta\rho$ are directly related to the yield ratio of light nuclei in heavy-ion collisions. To see the influence of the scalar-vector term on $y_2$, we evaluate its value in an infinitely quark matter of temperature $T = 30$ MeV at the end of its first-order phase separation. With the densities of the dense and dilute phases determined by the Maxwell's construction, the results for $y_2$ obtained with $G_{SV}$ equal to 0 and $-200 \, \Lambda^{-8}$ are shown in the lower panel of Fig. 4 by the solid and dashed lines, respectively, as a function of the averaged densities. It is seen that the $y_2$, hence the density inhomogeneity or fluctuation, is significantly larger for $G_{SV} = -200 \, \Lambda^{-8}$ than for $G_{SV} = 0$. Also, the density at which $y_2$ peaks shifts from $\rho \sim 0.53$ fm$^{-3}$ to $0.23$ fm$^{-3}$ when the value of $G_{SV}$ changes from zero to $G_{SV} = -200 \, \Lambda^{-8}$.

To search for the CEP, the beam energy scan program has been carried out at RHIC, with a particular emphasis on the possible nonmonotonic behavior of the fourth-order cumulant of net-proton multiplicity distribution as a function of collision energy, which has been assumed to be related to a similar behavior in the fourth-order quark number susceptibility of a thermally equilibrated QGP as it evolves towards its CEP as a result of the induced long-range correlations [63–65]. On the other hand, it has been suggested that the effects of the first-order phase transition in quark matter, which can lead to a large density inhomogeneity or fluctuation, could also be studied via cluster formation [57–59]. In particular, it has been shown that the first-order chiral phase transition in quark matter can result in an enhanced production of light nuclei in relativistic heavy-ion collisions [59]. For both observables, a detailed comparison between experimental data and theoretical results from the transport or hydrodynamic model is essential for extracting information on the QCD phase diagram from heavy-ion collisions in the beam energy scam program.

## B. The three-flavor NJL model

The three-flavor NJL model includes also the strange quark, which plays an important role in the partonic dynamic of heavy-ion collisions at high collision energies, The Lagrangian density in this model is given by [30]

$$\mathcal{L}_{\text{NJL}}^{\text{SU(3)}} = \mathcal{L}_0 + \mathcal{L}_S + \mathcal{L}_{SV} + \mathcal{L}_{\text{det}}, \quad (14)$$

with

$$\mathcal{L}_0 = \bar{\psi}(i\gamma^\mu \partial_\mu - \hat{m})\psi,$$

$$\mathcal{L}_S = G_S \sum_{a=0}^{8} [(\bar{\psi}\lambda^a \psi)^2 + (\bar{\psi}i\gamma_5 \lambda^a \psi)^2],$$

$$\mathcal{L}_{\text{det}} = -K[\det \bar{\psi}(1+\gamma_5)\psi + \det \bar{\psi}(1-\gamma_5)\psi], \quad (15)$$

where $\psi = (u, d, s)^T$ now represents the three-flavor quark fields and $\hat{m} = \text{diag}(m_u, m_d, m_s)$ is the corresponding current quark mass matrix. In the above, $\lambda^a (a = 1, ..., 8)$ with $\lambda^0$ being the identity matrix multiplied by $\sqrt{2/3}$ are the Gell-Mann matrices. The Lagrangian density $\mathcal{L}_{\text{det}}$ is the Kobayashi-Maskawa-t'Hooft (KMT) interaction [43] that breaks $U(1)_A$ symmetry with "det" denoting the determinant in the flavor space [66], i.e., $\det(\bar{\psi}\Gamma\psi) = \sum_{i,j,k}(\bar{u}\Gamma q_i)(\bar{d}\Gamma q_j)(\bar{s}\Gamma q_k)$. This term gives rise to six-point interactions in three flavors and is responsible for the flavor mixing effect. We assume in the present study that only $u$ and $d$ quarks can have the scalar-vector coupled interaction, so the term $\mathcal{L}_{\text{SV}}$ has the same form as in Eq. (2). Although this breaks the $SU(3) \times SU(3)$ symmetry in a specific way, a scalar-vector interaction term is still expected to be produced from quantum effects in the high momentum region of the nonperturbative renormalization group calculation of Ref. [47]. As in the case of the two-flavor NJL model, the value of $G_{\text{SV}}$ in the present study will be taken as a parameter to model the variation in the temperature and baryon chemical potential of the critical point of the quark matter.

In the mean-field approximation [56], the gap equations in the three-flavor NJL model for the quark in-medium effective masses, including that $(M_s)$ of strange quark, are given by

$$\begin{aligned}
M_u &= m_u - 4G_S\phi_u + 2K\phi_d\phi_s \\
&\quad - 2G_{\text{SV}}(\rho_u + \rho_d)^2(\phi_u + \phi_d), \\
M_d &= m_d - 4G_S\phi_d + 2K\phi_u\phi_s \\
&\quad - 2G_{\text{SV}}(\rho_u + \rho_d)^2(\phi_u + \phi_d), \\
M_s &= m_s - 4G_S\phi_s + 2K\phi_u\phi_d. \quad (16)
\end{aligned}$$

Besides the light quark condensates $\phi_u$ and $\phi_d$ as in the two-flavor NJL model, there is also the strange quark condensate given by

$$\phi_s = 2N_c \int \frac{d^3p}{(2\pi)^3} \frac{M_s}{E_s}(n_s^+ + n_s^- - 1), \quad (17)$$

where $n_s^\pm = [e^{\beta(E_s \mp \mu_s)} + 1]^{-1}$ with $E_s = (M_s^2 + \mathbf{p}^2)^{1/2}$ and $\mu_s$ being the strange quark chemical potential. The thermodynamic potential of the system can then be written as

TABLE II. Parameters in the three-flavor NJL model [30,39,40].

| $\Lambda$ [MeV] | $G_S\Lambda^2$ | $K\Lambda^5$ | $m_{u,d}$ [MeV] | $m_s$ [MeV] |
|---|---|---|---|---|
| 631.4 | 1.835 | 9.29 | 5.5 | 135.7 |

| $M_{u,d}$ [MeV] | $M_s$ [MeV] | $\langle \bar{u}u \rangle^{1/3}$ [MeV] | $\langle \bar{s}s \rangle^{1/3}$ [MeV] |
|---|---|---|---|
| 335 | 527 | −246.9 | −267 |

$$\begin{aligned}
\Omega_{\text{NJL}}^{\text{SU}(3)} &= 2G_S(\phi_u^2 + \phi_d^2 + \phi_s^2) + 3G_{\text{SV}}(\phi_u + \phi_d)^2(\rho_u + \rho_d)^2 \\
&\quad - 4K\phi_u\phi_d\phi_s - 2N_C \sum_{i=u,d,s} \int \frac{d^3p}{(2\pi)^3} E_i \\
&\quad - 2T \sum_{i=u,d,s} \int \frac{d^3p}{(2\pi)^3}(z^+(E_i) + z^-(E_i)). \quad (18)
\end{aligned}$$

To study the thermodynamic properties of a quark matter in the three-flavor NJL model, we employ the parameters $m_u = m_d = 5.5$ MeV, $m_s = 135.7$ MeV, $G_S\Lambda^2 = 1.835$, $K\Lambda^5 = 9.29$, and a cutoff $\Lambda = 631.4$ MeV [30], which are summarized in Table II together with the quark in-medium masses and condensates. The locations of the critical point in the temperature and baryon chemical obtained from the three-flavor NJL model with the scalar-vector coupled interaction are shown in Fig. 3 by the short dashed line. This line is almost identical to the solid line from the two-flavor NJL model except that the critical point in the three-flavor case moves to a higher temperature and smaller baryon chemical potential compared to the two-flavor case when the same $G_{\text{SV}}$ is used in the two calculations. The main reason for this similarity is because the parameters in the two-flavor and three flavor NJL models (see Tables I and II) give similar properties of the QCD vacuum, e.g., the quark condensates and in-medium masses. Results from these two models will not be identical if one uses different values for these parameters [30].

The scalar-vector term in the extended NJL Lagrangian shown in Eq. (14) respects the isospin symmetry but breaks the $SU(3)$ symmetry in flavor space. Since the $SU(3)$ flavor symmetry is already broken in the usual NJL Lagrangian by the much larger current mass of $s$ quark than those of $u$ and $d$ quarks, our approach preserves the same symmetries as the original NJL Lagrangian. Similar approaches have been adopted in the study of quark stars [67] and heavy-ion collisions [68–70] by introducing in the three-flavor NJL model additional scalar-isovector and vector-isovector interaction terms for $u$ and $d$ quarks with their strengths determined from empirical neutron star masses and radii as well as the isospin-dependent flow data from relativistic heavy ion collisions.

In principle, one can also include the scalar-vector coupled interactions for strange quarks. In this case, the dependence of the critical temperature on the value of $G_{\text{SV}}$ becomes much weaker than the results shown in the above. This is because the in-medium mass of strange quark is
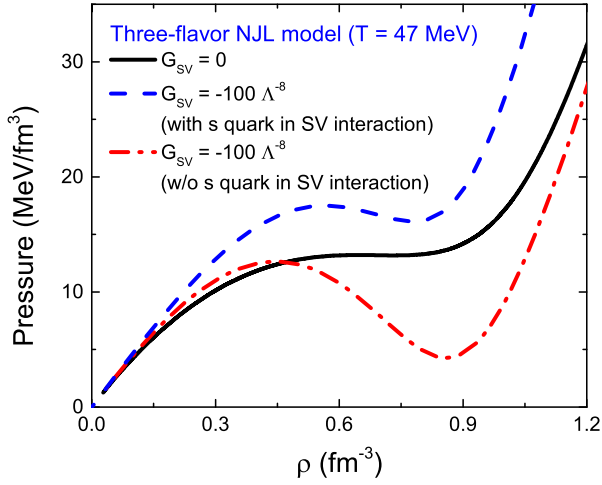
FIG. 5. Pressure as a function of net quark number density at temperature $T = 47$ MeV from the three-flavor NJL model for two different values of the scalar-vector (SV) coupling constant $G_{SV}$ and with and without including the strange quark in this interaction term.

much larger than the light quark masses, which makes it much harder for the quark matter to restore the spontaneously broken chiral symmetry. To quantify the effects of the scalar-vector interaction for strange quarks, we show in Fig. 5 the pressure of a quark matter at temperature $T = 47$ MeV as a function of its net-quark number density from the three-flavor NJL model. The red dash-dotted and blue dashed lines denote, respectively, the results from our approach and the approach including the strange quark scalar-vector interaction with the same coupling constant $G_{SV} = -100 \, \Lambda^{-8}$. Although the quark matter equation of state at densities $\rho = 0.5 - 0.8 \, \text{fm}^{-3}$, where $(\partial P/\partial \rho)_T \approx 0$ if $G_{SV} = 0$, is affected by the scalar-vector interaction in both approaches, the effect is much smaller in the case including the scalar-vector interaction for strange quarks. For $G_{SV} = -100 \, \Lambda^{-8}$, the critical temperature in our approach is increased from 47 MeV to 86 MeV, while it is only increased to 58 MeV if the strange quark scalar-vector interaction is also included. Therefore, allowing the scalar-vector interaction to act only on $d$ and $s$ quarks or $u$ and $s$ quarks would reduce the effect of this interaction on the temperature of the critical point.

## C. The NJL model with Polyakov loop

To include also the confinement-deconfinement phase transition, a constant temporal background gauge field representing the Polyakov loops $\Phi$ and $\bar{\Phi}$ has been added to the NJL model [20]. This so-called PNJL model changes the NJL Lagrangian density to

$$
\mathcal{L}_{PNJL} = \bar{\psi}(i\gamma^\mu D_\mu - \hat{m})\psi + \mathcal{L}_S + \mathcal{L}_{SV} \\
- \mathcal{U}(\Phi[A], \bar{\Phi}[A], T), \tag{19}
$$

where the covariant derivative is defined as $D^\mu = \partial^\mu - iA^\mu$ with $A^\mu = g\mathcal{A}_a^\mu(x)\lambda_a/2 \equiv \delta_0^\mu A_0$ being the $SU(3)$ gluon field in the Polyakov gauge and $g$ being the QCD strong coupling constant. Concerning the effective potential $\mathcal{U}$ for the Polyakov loops, various choices have been used in the literature [20,40,71–74]. In the present study, we adopted the following parametrization:

$$
\frac{\mathcal{U}(\Phi, \bar{\Phi}, T)}{T^4} = -\frac{1}{2}a(T)\bar{\Phi}\Phi \\
+ b(T)\ln[1 - 6\bar{\Phi}\Phi + 4(\bar{\Phi}^3 + \Phi^3) - 3(\bar{\Phi}\Phi)^2], \tag{20}
$$

with

$$
a(T) = a_0 + a_1\left(\frac{T_0}{T}\right) + a_2\left(\frac{T_0}{T}\right)^2, \\
b(T) = b_3\left(\frac{T_0}{T}\right)^3, \tag{21}
$$

where the parameters $a_0 = 3.51$, $a_1 = -2.47$, $a_2 = 15.2$, and $b_3 = -1.75$ are fitted to the results from the LQCD calculations of the thermodynamic properties of a pure gluon system [39,40]. For the temperature parameter $T_0$, its value is 270 MeV, corresponding to the critical temperature for the deconfinement phase transition of a pure gluon matter at zero baryon chemical potential [75]. The inclusion of quarks leads to a smaller value of $T_0 = 210$ MeV.

The grand potential of a quark matter at finite temperature and quark baryon potential in the PNJL model has a similar expression as Eq. (6) for the two-flavor or Eq. (18) for the three-flavor NJL model except the expression in Eq. (7) is replaced by

$$
z_\Phi^\pm = \ln[1 + 3(\bar{\Phi} + \Phi e^{-\beta(E_i \mp \mu_i^*)})e^{-\beta(E_i \mp \mu_i^*)} \\
+ e^{-3\beta(E_i \mp \mu_i^*)}]. \tag{22}
$$

As in the NJL model, the quark condensate and quark density are obtained by minimizing the grand potential, i.e., $\frac{\partial \Omega_{PNJL}^{SU(3)}}{\partial \phi_i} = \frac{\partial \Omega_{PNJL}^{SU(3)}}{\partial \rho_i} = 0$. Their expressions are similar to those given in Eqs. (10) and (11), except the color-averaged equilibrium quark occupation numbers $n_i^\pm$ are replaced by

$$
n_\Phi^\pm = \frac{\bar{\Phi}e^{2\beta(E \mp \mu^*)} + 2\Phi e^{\beta(E \mp \mu^*)} + 1}{e^{3\beta(E \mp \mu^*)} + 3\bar{\Phi}e^{2\beta(E \mp \mu^*)} + 3\Phi e^{\beta(E \mp \mu^*)} + 1}. \tag{23}
$$

From the above expression, one can see that the quark distribution retains the normal Fermi-Dirac form at high temperature when the Polyakov loops are $\Phi = \bar{\Phi} = 1$, while it becomes the Fermi-Dirac form with a reduced temperature $T/3$ at low temperature when $\Phi = \bar{\Phi} = 0$. Hence, the critical temperature in the PNJL model is generally higher than that in the NJL model as quarks in
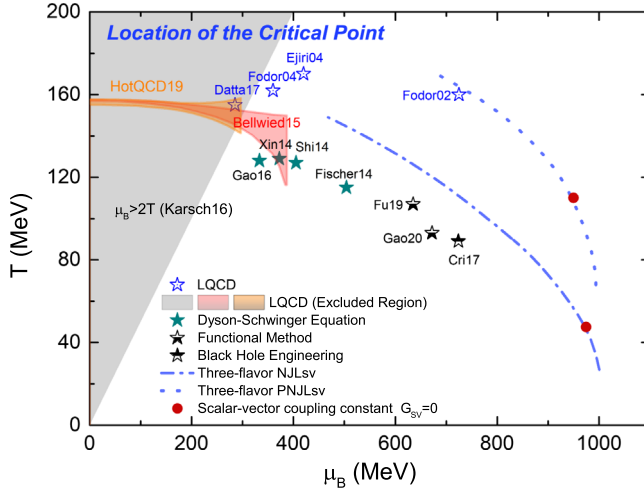
FIG. 6. Comparison of the location of the critical point in the plane of temperature $T$ versus baryon chemical potential $\mu_B$ from the three-flavor NJL (dash line) and PNJL (dotted line) models by varying the value of the scalar-vector coupling constant $G_{SV}$, with red solid circles denoting that obtained with $G_{SV} = 0$, with predictions from LQCD [76–82], Dyson-Schwinger equation [83–86], the functional renormalization method [87,88], and the method of black hole engineering [89].

PNJL model have a lower effective temperature. Note that the PNJL model at zero temperature is identical to the NJL model.

Minimizing the grand potential with respect to the Polyakov loops, i.e., $\frac{\partial\Omega^{SU(3)}_{PNJL}}{\partial\Phi} = \frac{\partial\Omega^{SU(3)}_{PNJL}}{\partial\Phi} = 0$, leads to the following mean-field equations for $\Phi$ and $\bar{\Phi}$ [68]:

$$\partial_\Phi\mathcal{U} = 6T\sum_{i=u,d,s}\int\frac{d^3p}{(2\pi)^3}\left[\frac{e^{-\beta(E_i-\mu_i^*)}}{\exp(z_\Phi^+(E_i))} + \frac{e^{-2\beta(E_i+\mu_i^*)}}{\exp(z_\Phi^-(E_i))}\right],$$

$$\partial_{\bar{\Phi}}\mathcal{U} = 6T\sum_{i=u,d,s}\int\frac{d^3p}{(2\pi)^3}\left[\frac{e^{-2\beta(E_i-\mu_i^*)}}{\exp(z_\Phi^+(E_i))} + \frac{e^{-\beta(E_i+\mu_i^*)}}{\exp(z_\Phi^-(E_i))}\right].$$

$$(24)$$

In Fig. 3, we show the locations of the critical point in the plane of temperature and baryon chemical potential obtained from both the two-flavor and the three-flavor PNJL model with the inclusion of the quark scalar-vector coupled interaction. As shown by the dashed line for the two flavor PNJL model and the dash-dotted line for the three-flavor NJL model, the effects of $G_{SV}$ are similar in these two cases. We also see that the effect of $G_{SV}$ on the critical chemical potential is smaller in the PNJL model than in the NJL model for both the two-flavor and the

three-flavor case. The effects of the scalar-vector interaction remain qualitatively the same for other choices of the Polyakov loop potential.

We further compare in Fig. 6 the critical point obtained from the three-flavor NJL (dash line) and PNJL (dotted line) models by varying the value of $G_{SV}$, with solid circles denoting those obtained with $G_{SV} = 0$, with selected predictions from LQCD [76–82], Dyson-Schwinger equation [83–86], the functional renormalization method [87,88], and the method of black hole engineering [89]. Predictions from other effective methods can be found in Refs. [23] and references therein. It is seen that with sufficiently attractive scalar-vector coupled interaction, the locations of the critical point in the NJL and PNJL models can be brought closer to those predicted from these first principle approaches.

## III. CONCLUSIONS

Based on the NJL model with both two flavors and three flavors as well as with the inclusion of Polyakov loops, we have studied the effect of the eight-quark scalar-vector coupled interaction, which has no effects on the QCD vacuum properties, on the critical end point of the first-order QCD phase transition line in the QCD phase diagram. We have found that the location of the critical point in the temperature and baryon chemical potential plane is very sensitive to the strength of this interaction and can be easily shifted by changing its value. This flexible dependence of the quark equation of state on its strength is useful for locating the phase boundary in QCD phase diagram by comparing the experimental data with results from transport model simulations [90] or hydrodynamic calculations based on equations of states from such generalized NJL and PNJL models. However, this flexibility hinges on the specific choice of the scalar-vector interaction in the SU(3) flavor space that it acts only on $u$ and $d$ quarks, although there is no evidence that this choice is realized in nature.

[1] P. Braun-Munzinger, V. Koch, T. Schäfer, and J. Stachel, Phys. Rep. **621,** 76 (2016).
[2] X. Luo and N. Xu, Nucl. Sci. Tech. **28,** 112 (2017).
[3] A. Bzdak, S. Esumi, V. Koch, J. Liao, M. Stephanov, and N. Xu, Phys. Rep. **853,** 1 (2020).
[4] M. A. Stephanov, Proc. Sci., LAT2006 (**2006**) 024 [arXiv: hep-lat/0701002].
[5] M. Nahrgang, Proc. Sci., CPOD2014 (**2015**) 032 [arXiv: 1510.08146].
[6] M. Bluhm *et al.*, Nucl. Phys. **A1003,** 122016 (2020).
[7] K. Murase and T. Hirano, Nucl. Phys. **A956,** 276 (2016).
[8] T. Hirano, R. Kurita, and K. Murase, Nucl. Phys. **A984,** 44 (2019).
[9] M. Nahrgang, M. Bluhm, T. Schäfer, and S. Bass, Acta Phys. Pol. B Proc. Suppl. **10,** 687 (2017).
[10] M. Bluhm, M. Nahrgang, T. Schäfer, and S. A. Bass, EPJ Web Conf. **171,** 16004 (2018).
[11] M. Singh, C. Shen, S. McDonald, S. Jeon, and C. Gale, Nucl. Phys. **A982,** 319 (2019).
[12] Y. Akamatsu, A. Mazeliauskas, and D. Teaney, Phys. Rev. C **95,** 014909 (2017).
[13] X. An, G. Basar, M. Stephanov, and H.-U. Yee, Phys. Rev. C **100,** 024910 (2019).
[14] M. Stephanov and Y. Yin, Phys. Rev. D **98,** 036006 (2018).
[15] K. Rajagopal, G. Ridgway, R. Weller, and Y. Yin, Phys. Rev. D **102,** 094025 (2020).
[16] C. Bernard, T. Burch, E. B. Gregory, D. Toussaint, C. E. DeTar, J. Osborn, S. Gottlieb, U. M. Heller, and R. Sugar (MILC Collaboration), Phys. Rev. D **71,** 034504 (2005).
[17] Y. Aoki, G. Endrodi, Z. Fodor, S. D. Katz, and K. K. Szabo, Nature (London) **443,** 675 (2006).
[18] A. Bazavov *et al.*, Phys. Rev. D **85,** 054503 (2012).
[19] M. Asakawa and K. Yazaki, Nucl. Phys. **A504,** 668 (1989).
[20] K. Fukushima, Phys. Rev. D **77,** 114028 (2008); **78,** 039902(E) (2008).
[21] S. Carignano, D. Nickel, and M. Buballa, Phys. Rev. D **82,** 054009 (2010).
[22] N. M. Bratovic, T. Hatsuda, and W. Weise, Phys. Lett. B **719,** 131 (2013).
[23] M. A. Stephanov, Prog. Theor. Phys. Suppl. **153,** 139 (2004); Int. J. Mod. Phys. A **20,** 4387 (2005).
[24] K. Fukushima and C. Sasaki, Prog. Part. Nucl. Phys. **72,** 99 (2013).
[25] G. Baym, T. Hatsuda, T. Kojo, P. D. Powell, Y. Song, and T. Takatsuka, Rep. Prog. Phys. **81,** 056902 (2018).
[26] Y. Nambu and G. Jona-Lasinio, Phys. Rev. **122,** 345 (1961).
[27] Y. Nambu and G. Jona-Lasinio, Phys. Rev. **124,** 246 (1961).
[28] T. Eguchi, Phys. Rev. D **14,** 2755 (1976).
[29] K. Kikkawa, Prog. Theor. Phys. **56,** 947 (1976).
[30] M. Buballa, Phys. Rep. **407,** 205 (2005).
[31] U. Vogl and W. Weise, Prog. Part. Nucl. Phys. **27,** 195 (1991).
[32] S. P. Klevansky, Rev. Mod. Phys. **64,** 649 (1992).
[33] T. Hatsuda and T. Kunihiro, Phys. Rep. **247,** 221 (1994).
[34] P. N. Meisinger and M. C. Ogilvie, Phys. Lett. B **379,** 163 (1996).
[35] P. N. Meisinger, T. R. Miller, and M. C. Ogilvie, Phys. Rev. D **65,** 034009 (2002).
[36] P. N. Meisinger, M. C. Ogilvie, and T. R. Miller, Phys. Lett. B **585,** 149 (2004).

[37] K. Fukushima, Phys. Lett. B **591,** 277 (2004).
[38] A. Mocsy, F. Sannino, and K. Tuominen, Phys. Rev. Lett. **92,** 182302 (2004).
[39] C. Ratti, M. A. Thaler, and W. Weise, Phys. Rev. D **73,** 014019 (2006).
[40] S. Roessner, C. Ratti, and W. Weise, Phys. Rev. D **75,** 034007 (2007).
[41] P. Costa, M. C. Ruivo, C. A. de Sousa, and H. Hansen, Symmetry **2,** 1338 (2010).
[42] J. Steinheimer and S. Schramm, Phys. Lett. B **736,** 241 (2014).
[43] G. 't Hooft, Phys. Rev. D **14,** 3432 (1976).
[44] A. A. Osipov, B. Hiller, and J. da Providencia, Phys. Lett. B **634,** 48 (2006).
[45] K. Kashiwa, H. Kouno, T. Sakaguchi, M. Matsuzaki, and M. Yahiro, Phys. Lett. B **647,** 446 (2007).
[46] A. A. Osipov, B. Hiller, J. Moreira, and A. H. Blin, Eur. Phys. J. C **46,** 225 (2006).
[47] K.-I. Aoki, K. Morikawa, J.-I. Sumi, H. Terao, and M. Tomoyose, Phys. Rev. D **61,** 045008 (2000).
[48] A. A. Osipov, B. Hiller, A. H. Blin, and J. da Providencia, Ann. Phys. (Amsterdam) **322,** 2021 (2007).
[49] A. A. Osipov, B. Hiller, and A. H. Blin, Eur. Phys. J. A **49,** 14 (2013).
[50] A. A. Osipov, B. Hiller, and A. H. Blin, Phys. Rev. D **88,** 054032 (2013).
[51] B. Hiller, J. Moreira, A. A. Osipov, and A. H. Blin, Phys. Rev. D **81,** 116005 (2010).
[52] J. Moreira, J. Morais, B. Hiller, A. A. Osipov, and A. H. Blin, Phys. Rev. D **91,** 116003 (2015).
[53] J. Moreira, J. Morais, B. Hiller, A. A. Osipov, and A. H. Blin, Phys. Rev. D **98,** 074010 (2018).
[54] V. Koch, T. S. Biro, J. Kunz, and U. Mosel, Phys. Lett. B **185,** 1 (1987).
[55] T.-G. Lee, Y. Tsue, J. da Providencia, C. Providencia, and M. Yamamura, Prog. Theor. Exp. Phys. **2013,** 013D02 (2013).
[56] U. Vogl and W. Weise, Prog. Part. Nucl. Phys. **27,** 195 (1991).
[57] J. Steinheimer and J. Randrup, Phys. Rev. Lett. **109,** 212301 (2012).
[58] J. Steinheimer, J. Randrup, and V. Koch, Phys. Rev. C **89,** 034901 (2014).
[59] K.-J. Sun, C. M. Ko, F. Li, J. Xu, and L.-W. Chen, arXiv:2006.08929.
[60] K.-J. Sun, L.-W. Chen, C. M. Ko, and Z. Xu, Phys. Lett. B **774,** 103 (2017).
[61] K.-J. Sun, L.-W. Chen, C. M. Ko, J. Pu, and Z. Xu, Phys. Lett. B **781,** 499 (2018).
[62] K.-J. Sun, C. M. Ko, and F. Li, arXiv:2008.02325.
[63] M. A. Stephanov, Phys. Rev. Lett. **102,** 032301 (2009).
[64] M. A. Stephanov, Phys. Rev. Lett. **107,** 052301 (2011).
[65] J. Adam *et al.* (STAR Collaboration), arXiv:2001.02852.
[66] M. Buballa, Phys. Rep. **407,** 205 (2005).
[67] P.-C. Chu, B. Wang, H.-Y. Ma, Y.-M. Dong, S.-L. Chang, C.-H. Zheng, J.-T. Liu, and X.-M. Zhang, Phys. Rev. D **93,** 094032 (2016).
[68] H. Liu, J. Xu, L.-W. Chen, and K.-J. Sun, Phys. Rev. D **94,** 065032 (2016).
[69] H. Liu and J. Xu, arXiv:1709.05178.

[70] H. Liu, F.-T. Wang, K.-J. Sun, J. Xu, and C. M. Ko, Phys. Lett. B **798**, 135002 (2019).

[71] C. Ratti, M. A. Thaler, and W. Weise, arXiv:nucl-th/0604025.

[72] S. K. Ghosh, T. K. Mukherjee, M. G. Mustafa, and R. Ray, Phys. Rev. D **77**, 094024 (2008).

[73] A. Bhattacharyya, S. K. Ghosh, S. Maity, S. Raha, R. Ray, K. Saha, and S. Upadhaya, Phys. Rev. D **95**, 054005 (2017).

[74] R. Stiele and J. Schaffner-Bielich, Phys. Rev. D **93**, 094014 (2016).

[75] M. Fukugita, M. Okawa, and A. Ukawa, Nucl. Phys. **B337**, 181 (1990).

[76] S. Ejiri, C. R. Allton, S. J. Hands, O. Kaczmarek, F. Karsch, E. Laermann, and C. Schmidt, Prog. Theor. Phys. Suppl. **153**, 118 (2004).

[77] Z. Fodor and S. D. Katz, J. High Energy Phys. 04 (2004) 050.

[78] S. Datta, R. V. Gavai, and S. Gupta, Nucl. Phys. **A904-905**, 883c (2013).

[79] F. Karsch *et al.*, Nucl. Phys. **A956**, 352 (2016).

[80] S. Datta, R. V. Gavai, and S. Gupta, Phys. Rev. D **95**, 054512 (2017).

[81] R. Bellwied, S. Borsanyi, Z. Fodor, J. Günther, S. D. Katz, C. Ratti, and K. K. Szabo, Phys. Lett. B **751**, 559 (2015).

[82] A. Bazavov *et al.* (HotQCD Collaboration), Phys. Lett. B **795**, 15 (2019).

[83] X.-y. Xin, S.-x. Qin, and Y.-x. Liu, Phys. Rev. D **90**, 076006 (2014).

[84] C. S. Fischer, J. Luecker, and C. A. Welzbacher, Phys. Rev. D **90**, 034022 (2014).

[85] C. Shi, Y.-L. Wang, Y. Jiang, Z.-F. Cui, and H.-S. Zong, J. High Energy Phys. 07 (**2014**) 014.

[86] F. Gao, J. Chen, Y.-X. Liu, S.-X. Qin, C. D. Roberts, and S. M. Schmidt, Phys. Rev. D **93**, 094019 (2016).

[87] W.-j. Fu, J. M. Pawlowski, and F. Rennecke, Phys. Rev. D **101**, 054032 (2020).

[88] F. Gao and J. M. Pawlowski, Phys. Rev. D **102**, 034027 (2020).

[89] R. Critelli, J. Noronha, J. Noronha-Hostler, I. Portillo, C. Ratti, and R. Rougemont, Phys. Rev. D **96**, 096026 (2017).

[90] F. Li and C. M. Ko, Phys. Rev. C **95**, 055203 (2017).